

Feasibility of a data-constrained prediction of shale microstructures

Yang Y. S.¹, **T. Gureyev**¹, **A. Tulloh**¹, **B. Clennell**² and **M. Pervukhina**²

¹ CSIRO Materials Science & Engineering, Private Bag 33, Clayton, Vic 3169, Australia

² CSIRO Petroleum Resources, PO Box 1130, Bentley, WA 6102, Australia

Email: Sam.Yang@csiro.au

Abstract: The microstructures of hydrocarbon reservoir shales and sandstones are critical in determining their permeability, mechanical, electrical and other physical properties. However, the available experimental techniques in characterising shale 3D microstructures are time consuming and sample destructive. This paper outlines our effort investigating the feasibility of determining shale microstructures using multiple computed-tomography (CT) data sets with different X-ray beam energies, together with a data-constrained microstructure (DCM) modelling approach. A sample composition data set was generated using an experimental tomography data set as a template for a shale rock sample with quartz, kaolinite and mica (illite). X-ray transmission through the sample was numerically simulated to produce X-ray projection images from the sample at multiple incident angles. This was repeated with several beam energies. The simulated projection images were used to reconstruct the 3D distribution of X-ray attenuation coefficient inside the sample for each energy. The compositional microstructures were predicted with our DCM software using the above 3D X-ray attenuation maps as constraints. Our preliminary comparisons indicate that the DCM-predicted compositional microstructure is qualitatively consistent with the known original microstructure. The accuracy of the prediction would depend on the CT reconstruction accuracy and the level of noise. Further work is in progress in quantitative evaluation of the predictions under various experimental conditions and rock microstructures.

Keywords: *Microstructure, data-constrained microstructure (DCM), computed tomography (CT), hydrocarbon reservoir, shale, sandstone*

1. INTRODUCTION

Microstructure is important in determining bulk properties of materials such as permeability, mechanical, electrical and other physical properties. Detailed knowledge of these properties is important in hydrocarbon reservoir exploration and well design [1]. Considerable efforts have been devoted to quantitative predictive modelling of microstructures [2-9]. However, the available experimental techniques for characterising 3D microstructure tend to be time consuming and sample destructive. A data-constrained microstructure (DCM) modelling approach and a software package have been developed which predicts sample-specific microstructures non-destructively [10-11]. It incorporates as constraints multiple computed-tomography (CT) data sets with different X-ray energies. In addition to CT data, X-ray energy-dependent attenuation properties and compositional sectional maps derived from such as X-ray scattering or SEM data can be used as a further constraint on the prediction.

DCM models a volume of material on a simple cubic lattice, where each site, or voxel, represents a small region of space containing a mixture of compositions forming the material. Voxel scale is determined by the input CT data resolution, which could be down to about 1µm. Each voxel stores the volume fraction (0-1) of each composition, including void (air). Also represented at each voxel are CT constraint data sets with different beam energies, in units of linear absorption coefficient (cm⁻¹). We refer to the compositions and CT data as ‘channels’ in the model.

To evaluate the feasibility of the DCM approach, a material sample with known microstructure is required. We started with known composition data and from this generated simulated CT data at a range of monochromatic beam energies. DCM was then used to predict the microstructure based on the simulated CT data. We were then able to compare the predicted composition to the known original.

2. SHALE ROCK SAMPLE DATA

A North Sea shale rock of Tertiary age was used as a testing sample. It consisted of weakly and randomly oriented clay minerals having a platy morphology, surrounded by angular quartz grains with sizes from less than 1µm up to 10µm across. The main minerals present were mica (illite), kaolinite and quartz, plus voids. X-ray micro-tomography was performed on a 1mm × 1mm × 5mm stick sample at the Argonne National Lab Advanced Photon Source in Chicago Illinois. The X-ray energy was 20keV. The simple mineralogy enabled the rock volume to be segmented approximately on the basis of the voxel intensity into the three mineral phases or void, using the constituent materials’ known X-ray attenuation coefficients. We then constructed a stack of 128 images of 512×512 pixels to represent the sample, where each pixel indicates the presence of only one of the three minerals or void. This compositional data was then used to generate simulated CT data for the sample at three X-ray energies: 25keV, 45keV and 65keV, at the same resolution. At each of the X-ray energies we calculated 360 projections over 180 degrees with 0.5 degrees angular step between projections. In order to calculate each projection, we computed line integrals through the sample, where each voxel's contribution was taken in accordance with the known X-ray attenuation value corresponding to one of the four materials and the given X-ray energy (Table 1). The computed projection data mathematically corresponds to the X-ray transform [12] of the simulated 3D sample. Subsequently, the calculated projections at each X-ray energy were

Table 1. Formulas, densities and total linear absorption coefficients of Quartz, Kaolinite, Mica (illite) and void at X-ray beam energies 25keV, 45keV and 65keV

Materials	Formulas	Densities (g/cm ³)	Total linear absorption coefficients (1/cm)		
			At 25keV	At 45keV	At 65keV
Quartz	SiO ₂	2.65	3.5497	0.98891	0.61424
Kaolinite	Al ₂ Si ₂ O ₅ (OH) ₄	2.60	3.0480	0.89604	0.58009
Mica (illite)	KAl ₂ (Si ₃ Al)O ₁₀ (OH) ₂	2.83	4.6826	1.2086	0.70605
Void		0	0	0	0

submitted to the conventional Filtered Back Projection (FBP) CT reconstruction algorithm which produced a 3D distribution of the X-ray attenuation coefficient at a given X-ray energy. Due to the inevitable reconstruction errors (related to the finite number of simulated projections, finite spatial resolution in each projection, etc.), the reconstructed 3D distributions of the X-ray attenuation coefficient differed from that in the original structure. The magnitude of these reconstruction errors was consistent with that expected in CT reconstruction from experimental data. In order to make our simulations even more realistic we added 1% simulated Poisson noise to the simulated X-ray projections. This allowed us to investigate the effect of

photon counting statistical noise on the accuracy of the reconstructed data, which is essential for planning of subsequent experiments. Finally, all data sets had their resolution reduced by a factor of four in all three dimensions to 128x128x32. An image on the y plane near the centre of the sample is shown in Figure 1. This was to provide a more challenging case, where voxels could now contain a mixture of compositions rather than a single type. Thresholding based on voxel image gray scale would become inadequate in determining the voxel compositions. CT images under different conditions, such as with different beam energies or different level of noise, are visually indistinguishable from Figure 1. A compositional image of the sample near its centre on the y plane is shown in Figure 2. Where a voxel contains a mixture of materials, colours are blended subtractively, approximating the mixing of paint on a white background.

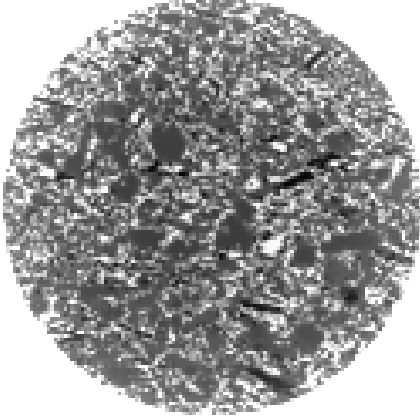


Figure 1. Re-sampled CT images of the shale rock sample at section 15 without added noise at beam energy 45 keV. Darker areas represent higher absorption.

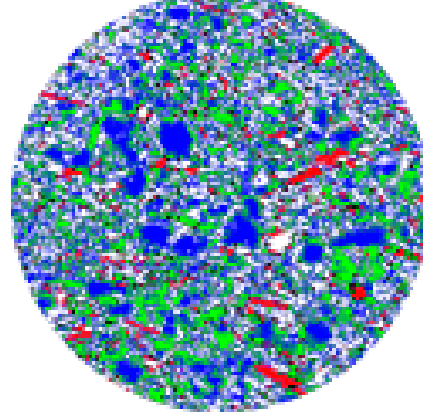


Figure 2. Re-sampled compositional map of the shale rock sample at section 15. Red: mica, Green: kaolinite, Blue: quartz..

3. MICROSTRUCTURE PREDICTION

In each voxel, the following assumptions have been made:

- The total volume of the voxel is the sum over the volumes of the individual compositions (including void) in the voxel.
- The total attenuation of an X-ray beam by the voxel is the sum over the attenuations of the individual compositions in the voxel.

The above assumptions can be expressed mathematically as

$$\left\{ \begin{array}{l} 0 \leq v_{\alpha,i} \leq 1 \\ \sum_{\alpha=0}^M v_{\alpha,i} = 1 \\ \bar{\mu}_i(\lambda_1) = \sum_{\alpha=0}^M v_{\alpha,i} \mu_{\alpha}(\lambda_1) \\ \bar{\mu}_i(\lambda_2) = \sum_{\alpha=0}^M v_{\alpha,i} \mu_{\alpha}(\lambda_2) \\ \vdots \\ \bar{\mu}_i(\lambda_L) = \sum_{\alpha=0}^M v_{\alpha,i} \mu_{\alpha}(\lambda_L) \end{array} \right. \quad (1)$$

where α ($\alpha = 0, 1, \dots, M$) denotes the compositions with M being the total number of compositions in the sample and $\alpha = 0$ corresponding to void; i ($i = 1, 2, \dots, N$) is the position index of a voxel, and N is the total number of voxels in the system; $v_{\alpha,i}$ is the volume-fraction of the α 'th composition at position i .

For an X-ray beam wavelength λ_j ($j=1,2,\dots,L$), $\bar{\mu}_i(\lambda_j)$ is the measured total linear absorption coefficient of the i 'th voxel, and $\mu_\alpha(\lambda_j)$ is the total linear absorption coefficient for the α 'th composition. Values for $\bar{\mu}_i(\lambda_j)$ can be derived from the CT data sets [12]. Values for $\mu_\alpha(\lambda_j)$ are available from, for example, handbooks of material properties [13]. In this article, it is assumed that the beam wavelength takes discrete values $\{\lambda_1, \lambda_2, \dots, \lambda_L\}$, where L is the total number of such 3D CT data sets. Monochromatic CT data sets can be obtained with synchrotron X-ray micro-tomography [14], or with more conventional X-ray equipment using appropriate filters and tube acceleration voltages. With polychromatic beams, the value $\mu_\alpha(\lambda)$ in Equation (1) would need to be replaced by an effective absorption coefficient which depends on the beam spectra and compositions [15].

In this article, the number of CT data sets with different beam energies is $L=3$, which is the same as the number of possible compositions $M=3$. Equation (1) yields a unique solution for compositional volume fractions $v_{\alpha,i}$ in all voxels. The solutions for all voxels form a predicted 3D compositional map of the original sample. Figure 3 shows section 15 of the predicted compositional map. Visual comparison of Figures 2 & 3 indicates that the DCM predicted microstructure is in reasonable agreement with the original structure. A slice near the centre of the sampled is selected for comparison as we expect the discrepancy would be largest there.

When 1% of simulated photon counting statistical noise is added, the CT images become noisy. This is particularly so for high X-ray beam energies, such as 65keV. One of the reasons is that at higher beam energy the sample becomes more transparent as beam attenuation by the sample is reduced. The attenuation of the sample is the imaging signal. Consequently, the signal to noise ratio is smaller for higher beam energy. The DCM predicted compositional microstructure with additional simulated noise is shown in Figure 4. The prediction error is significantly larger with the added noise.

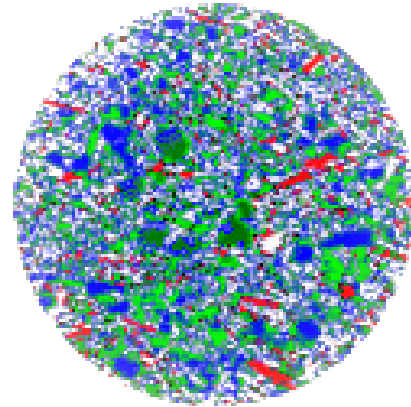


Figure 3. Compositional map of the DCM predicted shale rock sample at section 15 without simulated photon counting statistical noise. Red: mica, Green: kaolinite, Blue: quartz. Color blending is done as for Figure 2.

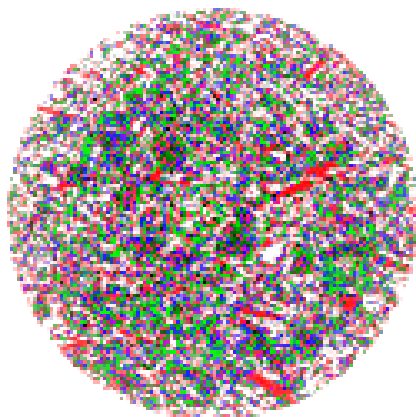


Figure 4. Compositional map of the DCM predicted shale rock sample at section 15 with 1% simulated photon counting statistical noise. Red: mica, Green: kaolinite, Blue: quartz. Color blending is done as for Figures 2 and 3.

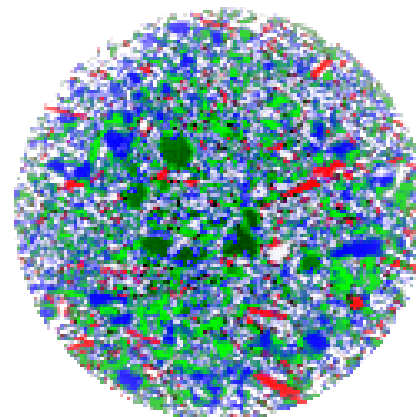


Figure 5. Compositional map of the DCM predicted shale rock sample at section 15 with 180 X-ray image projections over 180 degrees. Red: mica, Green: kaolinite, Blue: quartz. Color blending is done as for Figures 2-4.

CT reconstruction accuracy would be reduced with a smaller number of projection images. Figure 5 shows the predicted compositions on the same section using CT reconstructions with 180 projections over 180

degrees (1 degree angular step between projections) without simulated noise. Comparisons of Figures 2, 3 and 5 indicate that a smaller number of X-ray image projections give a less accurate composition prediction.

Visual comparisons of Figures 2 - 5 show that, as expected, the DCM prediction error is larger with added simulated noise. The figures also indicate that the DCM prediction would be biased towards compositions with higher attenuation coefficients.

In practice, the number of independent equations would be less than the number of compositions ($L < M$). This could be either due to the number of tomography data sets being less than the number of compositions of the system, or that some of the tomography data sets are linearly dependent on each other. For such a case, in general, there is a continuum of possible solutions for each voxel. All solutions from Equation (1) fall in the first hyper-octant which defines the physically possible solution space.

4. DISCUSSION AND CONCLUSIONS

The DCM approach shows promise as a technique for predicting microstructure, using CT data sets as constraints. However, its prediction accuracy depends on CT reconstruction accuracy and data noise level. We hope to further test and develop the algorithms using real CT data from sources such as the Australian Synchrotron. Future challenges include dealing with noise and polychromatic, rather than truly monochromatic X-ray energies; optimising the prediction algorithm; and microstructure-based predictions of bulk materials properties such as transport, thermal and electrical properties. As DCM requires high accuracy quantitative X-ray CT data, it would need more accurate quantitative calibrations of X-ray imaging equipment and CT reconstruction processes.

The current version of DCM software runs under 32 bit Microsoft Windows XP. We expect to port it to a higher performance computing platform in order to address memory and speed limitations inherent in the current platform.

ACKNOWLEDGMENTS

This work was sponsored by the CSIRO Computational and Simulation Science Transformational Capability Platform (CSS-TCP) and the CSIRO Wealth from Ocean Flagship (WfO).

REFERENCES

- [1] Di Maio, C. Hueckel, T. and Loret, B. eds., 2002. *Chemo-mechanical Coupling in Clays-From Nano-Scale to Engineering Applications*, Taylor and Francis, 339 pp.
- [2] G. Spanos (Eds), Viewpoint set no. 41: 3D Characterization and Analysis of Materials, *Scripta Materialia* **55** (2006) pp. 1-114.
- [3] R. D. MacPherson and D. J. Srolovitz, *Nature* **466** (2007) pp. 1053-1055.
- [4] S. Mourachov, *Computational Materials Science* **7** (1997) pp. 384-388.
- [5] D. Raabe, *Annu. Rev. Mater. Res.* **32** (2002) pp. 53-76.
- [6] A. L. Rohl, *Current Opinion in Solid State and Materials Science*, **7** (2003) pp. 21-26
- [7] T. Suzudo, *Physica A* **343** (2004) pp. 185-200.
- [8] Y. S. Yang, N. Blake, T. B. Abbott and J. F. McCarthy, *Scripta Metallurgica et Materialia* **29** (1993) pp. 1285-1290.
- [9] Y. S. Yang, N. Blake, T. B. Abbott and J. F. McCarthy, *Communications in Numerical Methods in Engineering* **11** (1995) pp. 805-812.
- [10] Y. S. Yang, A. Tulloh, I. Cole, S. Furman, A. Hughes, *International Conference and Exhibition - Materials and Austceram* (4-6 July 2007, Sydney Australia).
- [11] S. Yang, S. Furman and A. Tulloh, *Frontiers in Materials Science & Technology* (26 - 28 March 2008, Brisbane, Australia).

- [12] F. Natterer, *The Mathematics of Computerized Tomography*, John Wiley & Sons Ltd and B. G. Teubner, Stuttgart, 1989.
- [13] J. A. Ibers and W. C. Hamilton (Eds), *International Tables for X-ray Crystallography*, Vol IV. © International Union of Crystallography 1974.
- [14] J. Baruchel, J. Y. Buffiere, P. Cloetens, M. D. Michiel, E. Ferrie, W. Ludwig, E. Maire and L. Salvoc, *Scripta Materialia* **55** (2006) pp. 41–46.
- [15] T. E. Gureyev, D. M. Paganin, A. W. Stevenson, S. C. Mayo and S. W. Wilkins, *Phys. Rev. Lett.* **93** (2004) pp. 068103-1 – 068103-4.